

Effects of attractive and repulsive slit-pore confinement on the thermodynamics of an anomalous fluid

Fabio Leoni¹ and Giancarlo Franzese^{1,2}

¹*Departament de Física Fonamental i Departament de Física de la Matèria Condensada–Secció de Física Estadística i Interdisciplinar, Universitat de Barcelona, Martí i Franquès 1, 08028 Barcelona, Spain*

²*Institut de Nanociència i Nanotecnologia, Universitat de Barcelona, Av. Joan XXIII S/N, 08028 Barcelona, Spain**

(Dated: June 14, 2019)

Recent experiments and simulations have stimulated the debate about how confinement can change the thermodynamics of fluids with respect to the bulk case by enhancing or diminishing the crystallization rate at low temperature. An interesting case is water, for which confinement could be an experimental way to probe the supercooled fluid region—not accessible in bulk for the inevitable crystallization—if not pre-empted by heterogeneous crystallization. Here, we simulate the thermodynamics of eleven layers (~ 3.3 nm for water) of an anomalous fluid, with water-like properties, confined between a repulsive and an attractive wall, following our previous study about its structure and dynamics [J. Chem. Phys. 141, 174501 (2014)]. We find a broadening of the anomalous region and a liquid-liquid phase transition (LLPT) ending in a critical point with a shift of the characteristic temperature towards a higher value with respect to the bulk, in particular when the analysis does not exclude the portion of confined liquid that is heterogeneous (amorphous/crystal) at low temperature. Giving our results, we expect that the LLPT for water would become inaccessible in hydrophilic or hydrophobic slit pores of less than ~ 2.4 nm or ~ 1.2 nm, respectively, but would be accessible—at higher temperature with respect to bulk—in mild confinement, as in recent experiments by Zanotti et al. with Vycor glasses with 5 nm pore size, with consequences that could be relevant for applications in nanotechnology and biological systems.

* gfranzese@ub.edu

I. INTRODUCTION

Experiments and simulations have shown that fluids under geometrical nano-confinement present a different structural, dynamical and thermodynamical behavior respect to the bulk case. The study of such systems is relevant for their technological, experimental, and theoretical implications, e.g., [1–21]. Particularly interesting is the case of water, for which several experiments in confinement [22–31] have been interpreted as evidences of a liquid-liquid phase transition (LLPT), ending in a liquid-liquid critical point (LLCP), occurring in a range of temperatures where there is inevitable crystallization for bulk water [32]. This interpretation is possibly consistent with simulations [33–43] and theory [44, 45]. Alternative experimental interpretations, instead, suggest that any possible phase transition in confinement would be pre-empted by heterogeneous crystallization or by the appearance of heterogeneities (large variations) in the confined water density profile [46–48]. Here we investigate how confinement, by changing the crystallization rate, affects the thermodynamics of an anomalous fluid, with water-like properties, respect to the bulk case. We consider a fluid made of particles interacting through the Continuous Shouldered Well (CSW) potential [49–53], an isotropic pairwise core-softened interaction with a repulsive shoulder and an attractive well. This and other similar models have been used to describe globular proteins in solution [54], methanol hydroxyl groups [55], colloids [56, 57], liquid metals [52], liquid-liquid phase transition and water-like liquids [21, 50, 58–60]. In particular, the CSW reproduces density, diffusion and structure anomalies following the water hierarchy and displays a liquid-gas phase transition and a LLPT, both ending in critical points [50, 51]. In Ref. [53] we study by molecular dynamics (MD) simulations at constant volume V , temperature T and number of particles N the fluid between an attractive and a repulsive wall, parallel to each other in a slit-pore geometry. The attractive wall is made of immobile CSW particles in a triangular lattice, while the repulsive wall has no structure [53]. We find that the walls have an influence on the structure and the dynamics of the fluid, with a stronger effect near the attractive wall. In particular, CSW particles arrange in layers parallel to the walls, with large variations of density and structure among the layers. By decreasing T and increasing the density ρ we observe the formation of amorphous layers near the walls coexisting with the liquid. By further decreasing T we observe heterogeneous crystallization near the walls that extends toward the center of the pore as T decreases. We find that the structured attractive wall has an influence stronger than the repulsive wall thanks to a sequence of templating/molding/templating effects through the layers. Furthermore, we observe that the dynamics is largely heterogeneous among the layers and within the same layer at the interface with the walls.

Here we investigate the thermodynamics of the confined fluid. We find quantitative differences between isotherms calculated averaging only over the homogeneous fluid region and those calculated averaging over the entire system, including the amorphous or the crystal portion of the system inside the slit pore. However, we show that the two calculations are qualitatively consistent as long as there is a fluid region in the pore. In particular both calculations lead to a phase diagram with a LLPT ending in a critical point, as in bulk [49–51]. Furthermore, we observe a broadening of the anomalous region with a shift of characteristic densities and temperatures towards higher values.

II. METHODS

Particles of diameter equal to a interact through the CSW potential (inset Fig. 1) defined as [49]

$$U(r) \equiv \frac{U_R}{1 + \exp(\Delta(r - R_R)/a)} - U_A \exp\left[-\frac{(r - R_A)^2}{2\delta_A^2}\right] + \left(\frac{a}{r}\right)^{24} \quad (1)$$

where $R_A/a = 2$ and $R_R/a = 1.6$ are the distance of the attractive minimum and the repulsive radius, respectively, U_A and U_R are the energies of the attractive well and the repulsive shoulder, respectively, with $U_R/U_A = 2$, $(\delta_A/a)^2 = 0.1$ is the variance of the Gaussian centered in R_A and $\Delta = 15$ is the parameter which controls the slope between the shoulder and the well at R_R . In order to reduce the computational cost, we impose a cutoff for the potential at a distance $r_c/a = 3$. The parameters employed are the same as in Refs.[49–53]. Particles are confined between two parallel walls separated along the z axis by a fixed distance $L_z/a = 19$. We consider a NVT ensemble composed of $N = 1024$ particles for the confined case, and $N = 676$ particles for the bulk case, at fixed temperature T and volume V . The value N for the bulk is chosen in such a way to be comparable with the typical number of particles in the homogeneous region of the fluid in the confined case (corresponding to the cyan regions of the density profile in Fig.1 of Ref. [53]). Comparisons of our results for the bulk with $N = 676$ particles with those in literature for $N = 1372$ [51, 52] show no relevant size effects. Pressure, temperature, density, diffusion constant and time are all expressed in internal units: $P^* \equiv Pa^3/U_A$, $T^* \equiv k_B T/U_A$, $\rho^* \equiv \rho a^3$, $D^* \equiv D(m/a^2 U_A)^{1/2}$, and $t^* \equiv (a^2 m/U_A)^{1/2}$, respectively, with a unit of distance. For sake of simplicity, in the following we will drop all the * denoting internal units. We adopt periodic boundary conditions in the x and y directions. In order to compute the effective density ρ_{eff} , we calculate

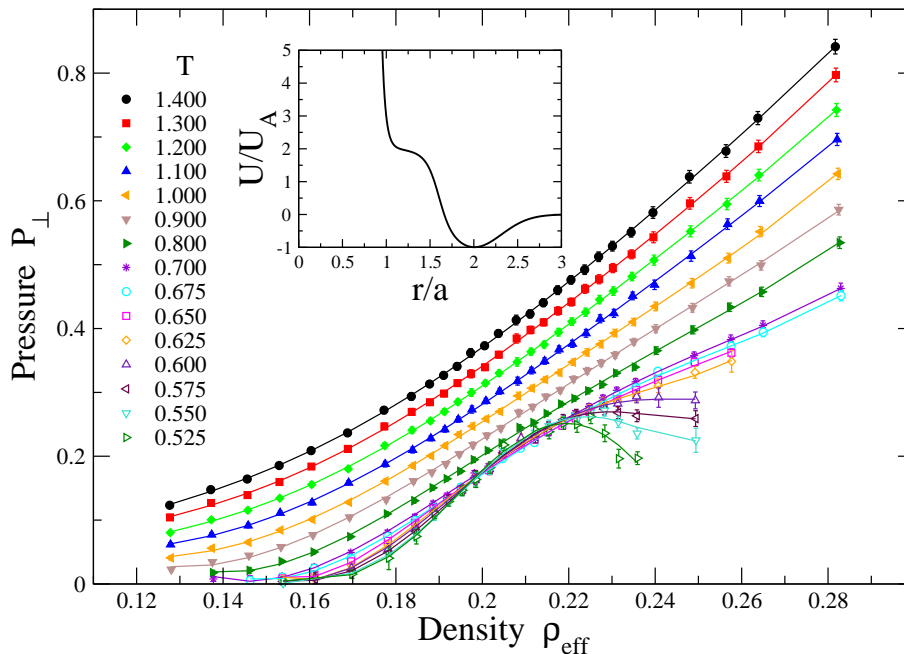


FIG. 1. Isotherms in the $P_{\perp} - \rho_{\text{eff}}$ phase diagram for the CSW fluid confined in a slit pore, from $T = 1.400$ (top) to $T = 0.525$ (bottom). The normal pressure P_{\perp} is always positive for all densities. Inset: the CSW interparticle potential.

the effective volume V_{eff} accessible to particles $V_{\text{eff}} \equiv L_z^{\text{eff}} A$, where $A \equiv L_x L_y$ is the section of the simulation box and L_z^{eff} is the effective distance between the plates. By considering the quenched particles forming the attractive wall and the interaction with the repulsive wall, we obtain $L_z^{\text{eff}} \simeq L_z - a/2 - (1/T)^{1/9}$ [61]. The effective density is $\rho_{\text{eff}}(\rho, T) \equiv \rho L_z / L_z^{\text{eff}}$ with $\rho_{\text{eff}} \lesssim 1.08\rho$ for all the state points considered here. For the sake of minimizing finite-size effects when we compare results for different densities, we keep N constant and change L_x and L_y for fixed L_z . All our results are averaged over 10 independent samples for the confined fluid, and over 4 independent samples for the bulk.

III. RESULTS AND DISCUSSION

A. The phase diagram for the confined fluid

In order to check the stability of the system corresponding to a specific thermodynamic state (N, V, T) , we verified that the energy and the pressure are equilibrated, as discussed in Ref. [53]. In inhomogeneous systems, as nano-confined fluids, the tensorial nature of the pressure has to be taken into account [61]. For confinement in a slit pore geometry the parallel pressure is $P_{\parallel}(z) \equiv P_{xx}(z) \equiv P_{yy}(z)$ and the normal pressure is $P_{\perp} = P_{zz} = \text{const.}$, while the nondiagonal components of the pressure tensor are zero (no shear forces are present in the fluid) [61, 62]. The normal pressure P_{\perp} (Fig. 1) can be computed as the net force along the z axis per unit area acting on one of the walls [53]. Consistent with the mechanical equilibrium, we verify that P_{\perp} does not depend on the z coordinate, with $P_{\perp} \geq 0$ for all densities [53].

In slit pore geometries the parallel pressure plays the role of the isotropic bulk pressure [44, 62]. We calculate P_{\parallel} for two different portions of the system: (i) for the homogeneous liquid and (ii) for the entire ensemble of particles inside the pore, including the heterogeneous part. The calculation (i) corresponds to the correct quantity that should be compared with the (homogeneous) bulk fluid case. The calculation (ii) is the one that is usually performed in experiments and, for the sake of comparison with experiments, in several computational works. In both cases we use the virial expression for the x and y directions [63]

$$P_{\parallel} \equiv k_B T \rho - \frac{1}{2V} \left\langle \sum_i \sum_{j>i} \frac{x_{ij}^2 + y_{ij}^2}{r_{ij}} \left(\frac{\partial U(r)}{\partial r} \right)_{r=r_{ij}} \right\rangle \quad (2)$$

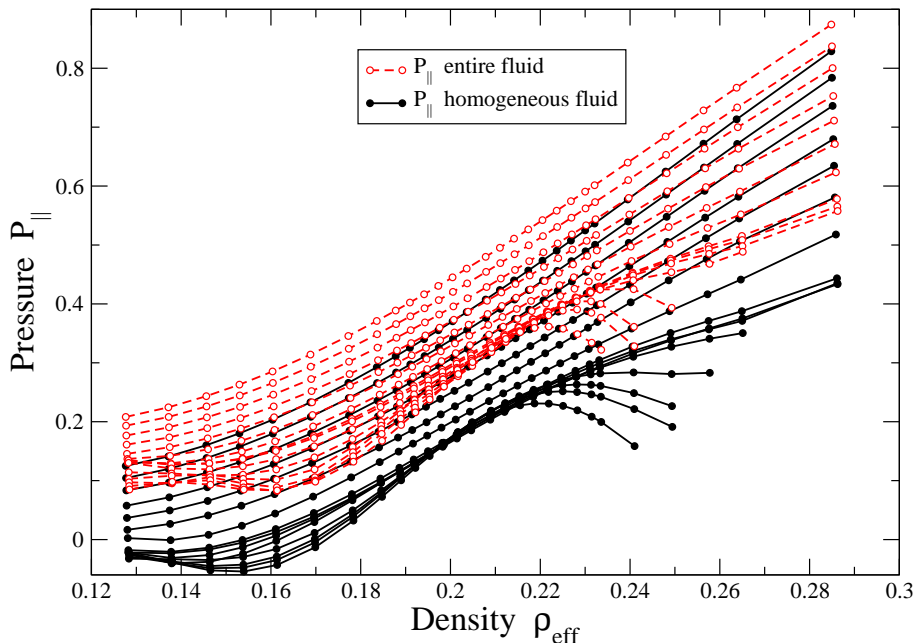


FIG. 2. Isotherms in the $P_{\parallel} - \rho_{\text{eff}}$ phase diagram for the CSW fluid confined in a slit pore for the homogeneous liquid part of the system (full symbols with continuous black lines) or for the entire ensemble of particles inside the pore, including the heterogeneous part (open symbols with dashed red lines). In both sets, isotherms are, from top to bottom, the same reported in Fig. 1. We find that isotherms describing the entire ensemble respect to the homogeneous liquid are shifted towards higher pressures, especially at lower densities.

where k_B is the Boltzmann constant and $r_{ij} \equiv |\vec{r}_i - \vec{r}_j|$.

We find that the isotherms for the calculation (ii) are shifted towards higher pressures respect to those for the calculation (i), especially at lower densities (Fig. 2). We understand this effect as a consequence of the density heterogeneities in the system due to the layering. As seen in Fig.1 of Ref. [53], the density profile $\rho(z)$ has large variations near the walls, especially close to the attractive wall, reaching values that are also ten times larger than the average density. Hence, within this heterogeneous region the inter-particles distance can be largely reduced with respect to the homogeneous fluid, inducing large repulsive contributions to the average P_{\parallel} for the Eq. (2). Because the local density in the homogeneous fluid is slightly smaller (larger) than ρ_{eff} at low (high) density, with a deviation—never larger than 8%—that decreases for increasing ρ , we observe a decrease of the difference between P_{\parallel} for the two calculations (i) and (ii) for our state points (Fig. 2). From now on we will refer to P_{\parallel} as the one resulting from the calculation (i), i.e., over the homogeneous fluid.

B. Comparison of the confined and bulk phase diagrams

Next, we compare the phase diagram of the homogeneous confined fluid with the bulk (Figs. 3 and 4). We observe that for densities $\sim 0.13 \div 0.19$ bulk isotherms are more separated in pressure with respect to their confined counterparts. However, we find a partial qualitative agreement because in both systems we observe the occurrence of isotherms whose density-derivative smoothly changes from positive to negative in two well separated density intervals, below and above density ~ 0.16 . Based on our detailed knowledge of the phase diagram for the bulk system [50, 51], we identify these two regions with the gas-liquid coexistence at lower densities and the liquid-liquid coexistence at higher densities. We approximate the gas-liquid (C_1) and the liquid-liquid (C_2) critical points with the state points at the highest T where the density-derivative along the isotherm is approaching zero below and above density ~ 0.16 , respectively. From the calculations in Figs. 3 and 4, we estimate the critical parameters as in Table I. We do not find any significant difference, within our numerical precision, between the estimated parameters.

To make a better comparison, we apply a linear transformation to the entire set of isotherms of the bulk, $\rho_{\text{tr}} \equiv a(T)\rho + b(T)$ and $P_{\text{tr}} \equiv c(T)P + d(T)$ where a , b , c , d are linear functions of the temperature, $a(T) \equiv a_0T + a_1$ etc.,

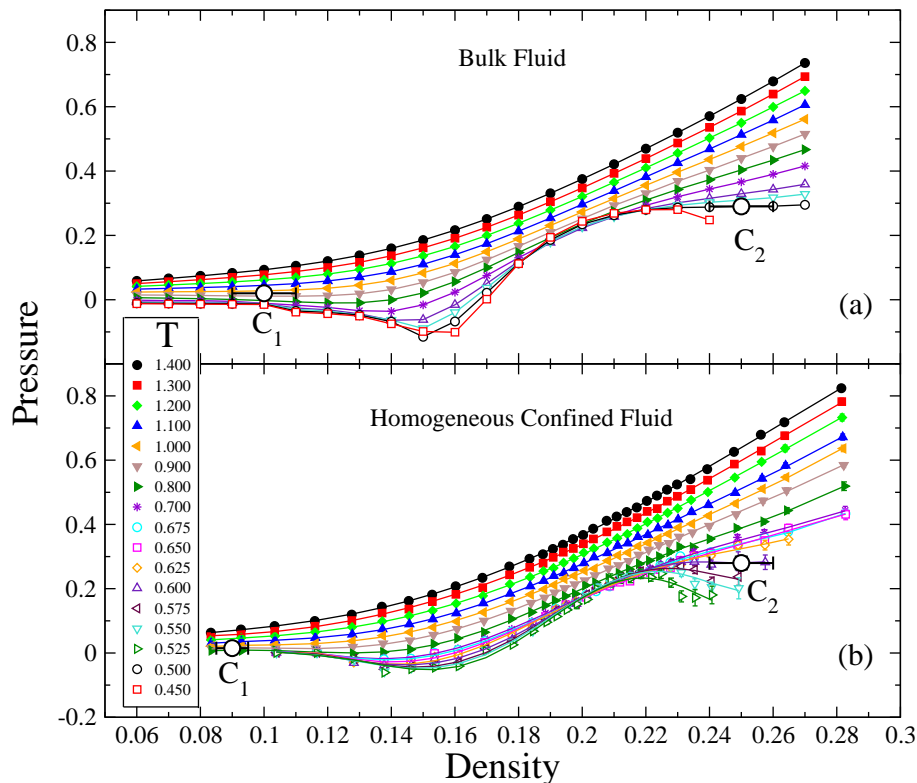


FIG. 3. Comparison between the phase diagrams of the bulk and confined fluids. (a) Isotherms in the $P - \rho$ plane of the bulk fluid and (b) in the $P_{\parallel} - \rho_{\text{eff}}$ plane of the homogeneous liquid confined in a slit pore. In both panels isotherms are between $T = 1.4$ (top) and $T = 0.45$ (bottom). Open symbols with error bars and labels C_1 and C_2 denote our estimates for the gas-liquid and the liquid-liquid critical point, respectively.

	Density C_1	Pressure C_1	Temp. C_1	Density C_2	Pressure C_2	Temp. C_2
Bulk	0.100 ± 0.010	0.020 ± 0.015	0.94 ± 0.05	0.25 ± 0.01	0.29 ± 0.02	0.50 ± 0.05
Confined	0.090 ± 0.005	0.015 ± 0.015	0.90 ± 0.05	0.25 ± 0.01	0.28 ± 0.02	0.59 ± 0.02

TABLE I. Estimates of the parameters for the gas-liquid critical point C_1 and the liquid-liquid critical point C_2 for the bulk fluid (upper row) and the homogeneous confined fluid (lower row).

and we minimize with respect to the T -independent coefficients, a_0, a_1 etc., the cumulative deviation

$$\delta \equiv \sum_i \delta_i \equiv \sum_i \left[\int_{\rho_{\min}}^{\rho_{\max}} (P_{\text{tr}}(T_i) - P_{\parallel}(T_i))^2 d\rho \right]^{1/2}, \quad (3)$$

where T_i refers to the temperature of the i -th isotherm, and ρ_{\min} and ρ_{\max} are the minimum and maximum density, respectively, for the considered range of comparison between the two phase diagrams (Fig. 5).

The transformation allows us to almost superimpose the two phase diagrams at high temperatures, but show deviations at low T . Therefore, our results suggest that, although the two phase diagrams are qualitative similar, is not possible to find an exact mapping of one onto the other. This observation could be relevant when experimental data for confined fluids are compared to the corresponding bulk system.

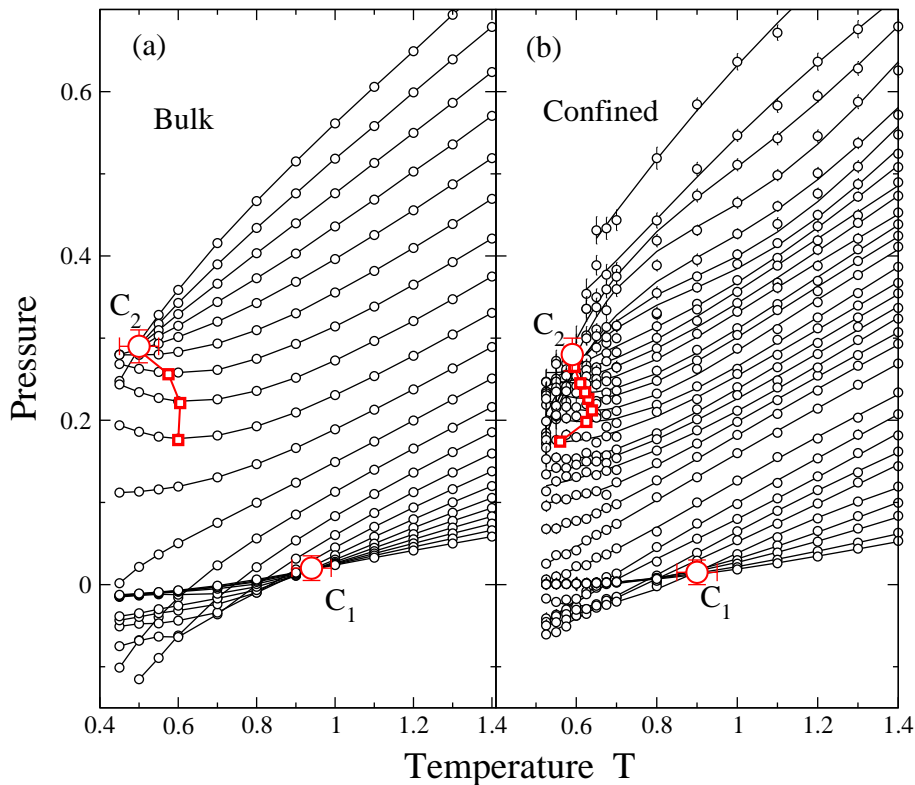


FIG. 4. The pressure-temperature phase diagram emphasizes the density anomaly. The line of Temperature of Maximum Density (TMD) corresponds to the minima (red squares) along isochores (circles connected by lines) in the P - T plane for bulk (a), and in P_{\parallel} - T plane for the confined fluid (b). Isochores in panel (a) are for densities from 0.27 (top at $T = 1.3$) to 0.06 (bottom at $T = 1.3$) with 0.01 decrease in density from one isochore to the next. In panel (b) the top isochore at $T = 1.4$ is for $\rho_{\text{eff}} \simeq 0.281$ and the bottom for $\rho_{\text{eff}} \simeq 0.083$ with $\simeq 0.01$ decrease in density from one isochore to the next. In both panels C_1 and C_2 (large red circles) mark the gas-liquid and liquid-liquid critical points, respectively.

C. Temperature of maximum density

A remarkable anomaly of water and other anomalous liquids is the occurrence of minima along isochores in the pressure-temperature plane indicating the presence of a line of Temperatures of Maximum Density (TMD) for the fluid at fixed pressure. The CSW fluid displays a TMD line in bulk (Fig. 4.a) [50, 51]. Here we find the occurrence of this anomaly also for the confined CSW fluid. For a number of isochores we observe minima and, by calculating numerically $(\partial P_{\parallel} / \partial T)_{\rho} = 0$, we identify the TMD line (Fig. 4.b). We observe that for densities $\gtrsim 0.2$ the TMD line slightly moves toward higher T for the confined case, but that in both bulk and confined fluid the TMD line converges toward the liquid-liquid critical point C_2 in the pressure-temperature plane. diagram.

D. Structural anomaly

Another anomaly that characterizes water and other anomalous liquids is the non-monotonic behavior of parameters that quantify the structural order in the fluid. In particular, the translational order can be estimated by the parameter [64–66]

$$t \equiv \int_0^{\infty} |g(\xi) - 1| d\xi \quad (4)$$

where $\xi \equiv r\rho^{1/3}$ is the distance r in units of the mean interparticle separation $\rho^{-1/3}$ and $g(\xi)$ is the radial distribution function that by definition is proportional to the probability of finding a particle at a distance ξ from a reference

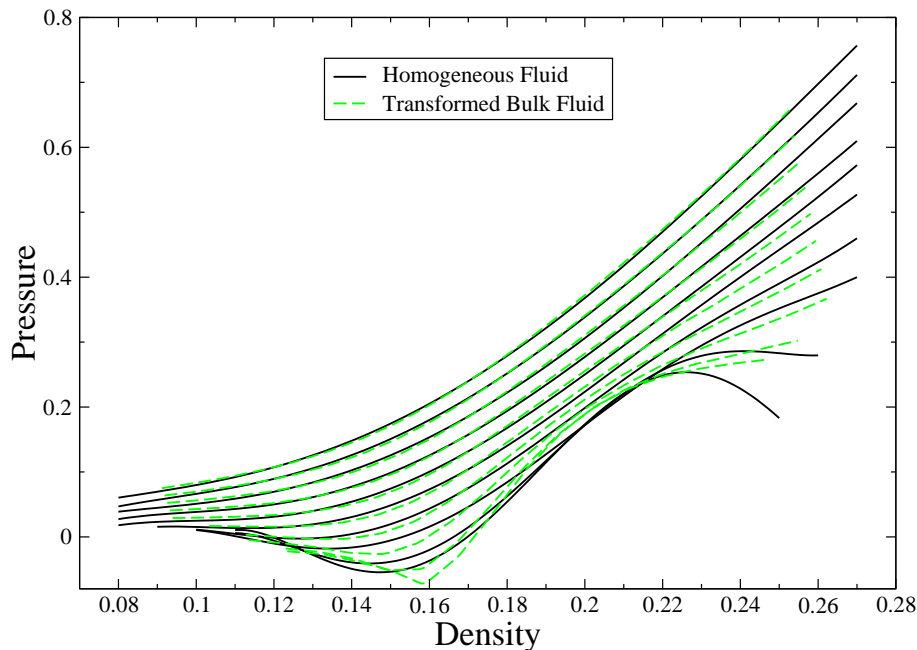


FIG. 5. A global transformation allows us to compare the phase diagram of the bulk and the confined fluids. Isotherms of the confined homogeneous fluid (continuous black lines) and the bulk fluid after the global transformation (dashed green lines) are from $T = 1.4$ (top) to 0.55 (bottom). The transformation coefficients are $a_0 = -0.02$, $a_1 = 0.912$, $b_0 = 0.00$, $b_1 = 0.02$, $c_0 = -0.02$, $c_1 = 1.12$, $d_0 = -0.02$, $d_1 = 0.02$.

particle. For an ideal gas it is $g(\xi) = 1$ at any distance and there is no translational order ($t = 0$). For normal fluids t increases monotonically for increasing density along isotherms. For anomalous liquids there is a range of densities and temperatures within which t decreases for increasing density along isotherms, indicating that the translational order is progressively reduced until reaching a minimum value before recovering a normal, increasing, behavior [52, 65]. Because the CSW fluid displays this structural anomaly in the bulk [50, 51] we investigate how the confinement affects this property. In particular, we calculate t by numerical integration of $|g(\xi) - 1|$ up to a cutoff distance ξ_c set to half of the simulation box times $\rho^{-1/3}$ because in our simulations for $\xi > \xi_c$ it is $g(\xi) \simeq 1$. We find that t is monotonically increasing for $T \geq 1.8$ (not shown), while for lower T it has maxima and minima delimiting an anomalous region (Fig. 6). Comparing with the bulk (Fig. 6, inset), we observe that for the confined fluid the anomaly extends at higher T and larger ρ .

E. Diffusion anomaly

Next we study diffusion properties of the confined fluid and compare it with the bulk case (Fig. 7). In bulk there is a density region at low enough T within which the diffusion coefficient displays an anomalous increase for increasing density. In normal fluids, the diffusion coefficient monotonically decreases for increasing density along isotherms.

To define correctly the diffusion constant in the confined case it is necessary (i) to reach the diffusion regime for the mean square displacement (MSD) and (ii) to be sure that the particles explore an environment that is homogeneous over the diffusion time-scale, otherwise the heterogeneities that survive over large time-scales could lead to apparent superdiffusive or subdiffusive regimes [53]. Condition (i) can be satisfied thanks to our set-up with periodic boundary conditions parallel to the walls, while to guarantee condition (ii) we focus on those particles that moves only within the region of the slit pore where the liquid phase is homogeneous (see Fig.1 of Ref. [53]). For them we define the MSD parallel to the walls as [53]

$$\langle (\Delta r_{\parallel}(\tau))^2 \rangle \equiv \langle (r_{\parallel}(t - t_0) - r_{\parallel}(t_0))^2 \rangle, \quad (5)$$

where $\tau \equiv t - t_0$ is the time spent in the homogeneous region of the pore by a particle that stays or enters in this region at time t_0 , and $r_{\parallel} \equiv (x^2 + y^2)^{1/2}$. The diffusion coefficient D_{\parallel} in the direction parallel to the walls is by

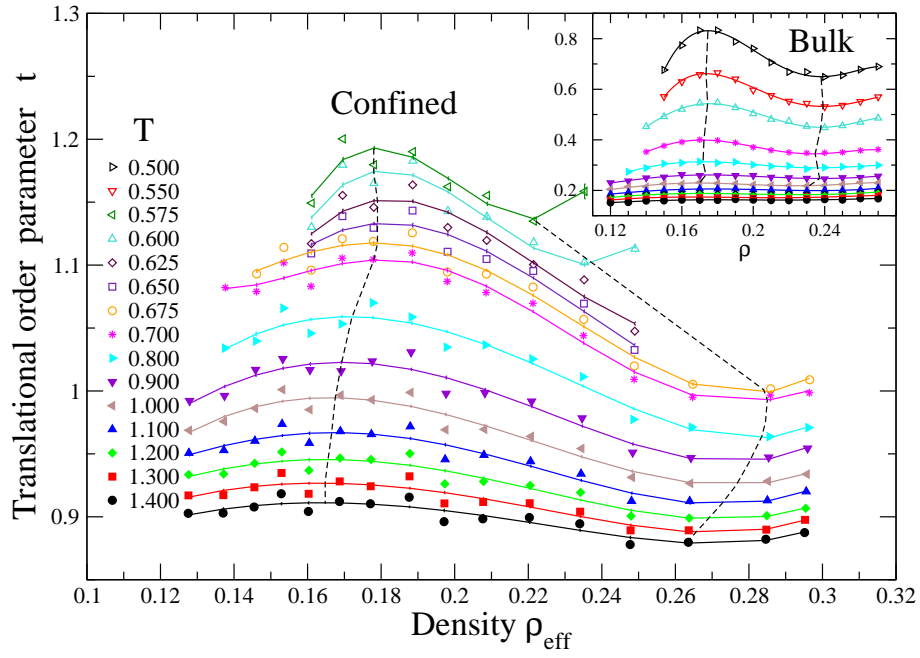


FIG. 6. Translational Order Parameter t for the homogeneous fluid confined in a slit pore from $T = 0.575$ (top) to $T = 1.4$ (bottom). Inset: t for the bulk from $T = 0.5$ (top) to $T = 1.4$ (bottom). In both panels dotted lines are guides for the eyes delimiting the anomalous region where t decreases for increasing density.

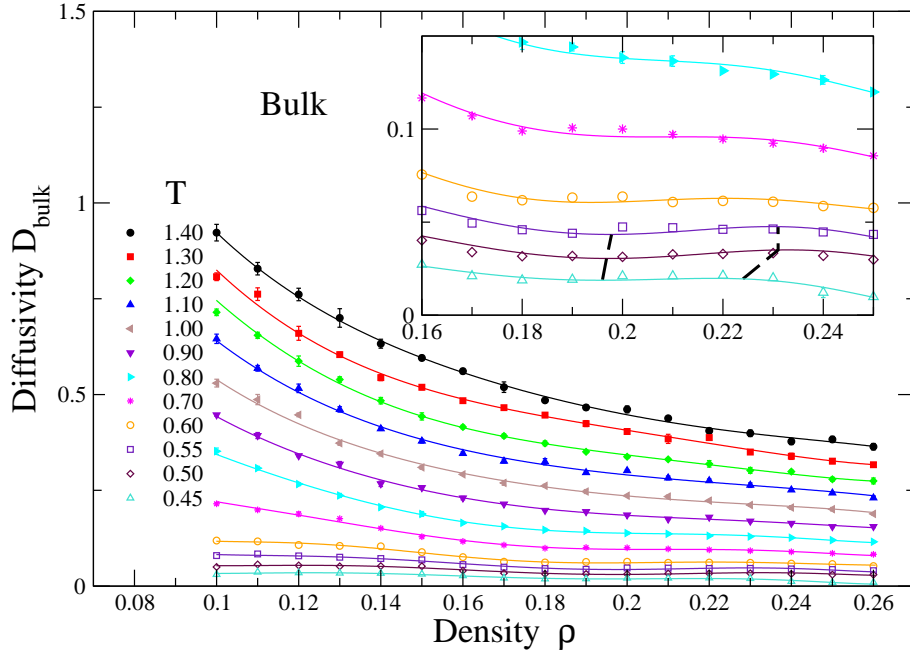


FIG. 7. The diffusion coefficient D_{bulk} for the bulk fluid has an anomalous behavior at low T and intermediate density. Calculations are for isotherms going from $T = 0.45$ (bottom) to $T = 1.4$ (top). Inset: Isotherms from $T = 0.45$ (bottom) to $T = 0.8$ (top). The dashed black lines delimit the anomalous region where D_{bulk} increases for increasing density.

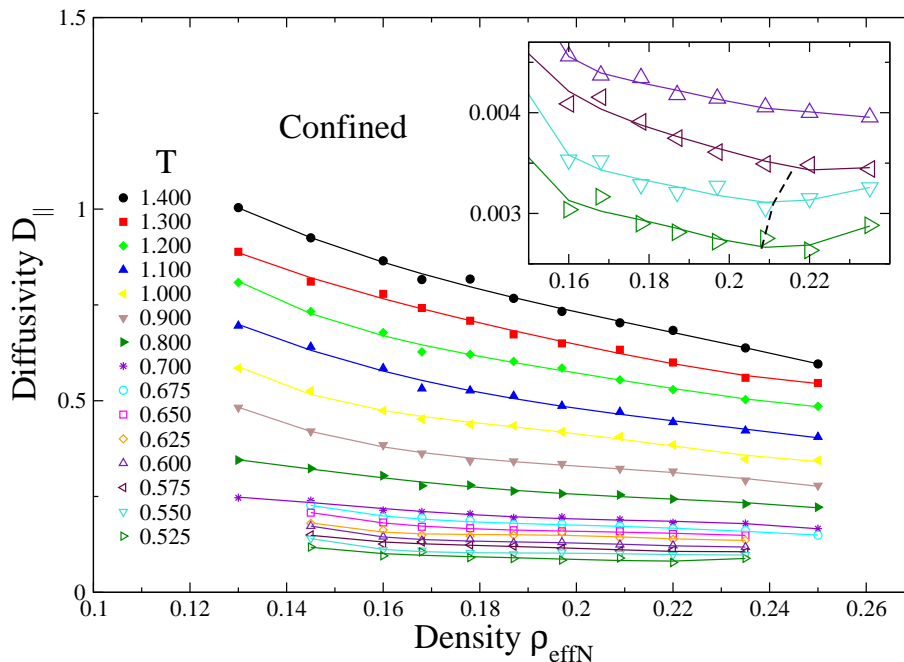


FIG. 8. Diffusion coefficient D_{\parallel} for the confined homogeneous fluid. Calculations are for isotherms from $T = 0.525$ (bottom) to $T = 1.4$ (top) for the homogeneous confined fluid. Inset: Isotherms, from $T = 0.525$ (bottom) to $T = 0.6$ (top), for which a minimum D_{\parallel}^{\min} (marked by the dashed black line) of D_{\parallel} is clearly observable. For $\rho \geq \rho(D_{\parallel}^{\min})$ the diffusion is anomalous. Our data do not allow us to estimate where, for these isotherms, the region of anomalous diffusion ends.

definition a constant given by

$$D_{\parallel} \equiv \lim_{\tau \rightarrow \infty} \langle (\Delta r_{\parallel}(\tau))^2 \rangle / (4\tau). \quad (6)$$

In Ref. [53] we analyzed the MSD layer by layer as a function of temperature and density and discussed the consequences of including heterogeneous regions in the calculations. Here, we extract from the data for the homogeneous region the behavior of the diffusion coefficient D_{\parallel} along isotherms as a function of the system density (Fig. 8). For $T \geq 0.625$ we do not observe any diffusion anomaly with D_{\parallel} monotonically decreasing for increasing density. Instead, for $0.525 \leq T \leq 0.600$ we find that D_{\parallel} behaves as a normal fluid for $\rho_{\text{eff}} \lesssim 0.21$, reaches a minimum D_{\parallel}^{\min} at $\rho_{\text{eff}} \simeq 0.215$, and displays an anomalous increase for $\rho_{\text{eff}} \gtrsim 0.22$. Comparing Figs. 7 and 8 we observe that the diffusion anomaly in the confined systems starts at higher densities and higher temperatures with respect to the bulk case. Although we expect to observe a regular behavior of D_{\parallel} for higher density as in bulk, the inevitable amorphization and heterogeneous crystallization of the confined fluid at higher density and low T [53] does not allow us to specify where the region of anomalous diffusion ends.

IV. SUMMARY AND DISCUSSION

We study by MD simulations how the geometrical nano-confinement of the CSW anomalous fluid in a slit pore with an attractive wall and a repulsive wall affects the phase diagram and the occurrence of the anomalies. In a previous work [53] we found that the slit pore has a drastic effect on the structural and dynamical properties of the system. At low density (low hydration), the fluid accumulates mainly on the attractive wall leaving no free fluids, especially at low T . At intermediate and high density the attractive wall has a long-range influence on the fluid, despite we set the wall to a structure that does not correspond to a crystalline energy minima for the CSW potential within the considered densities. The attractive wall induces a sequence of templating–molding–templating effects on the nearest layers of the confined fluid, favoring the heterogeneous nucleation of the crystal at low T and limiting the possibility to have free fluid in the pore. On the other hand, the repulsive wall has a weak effect on the structure for the considered T and ρ . Overall, the confinement reduces the P - ρ region where the free fluid has a homogeneous

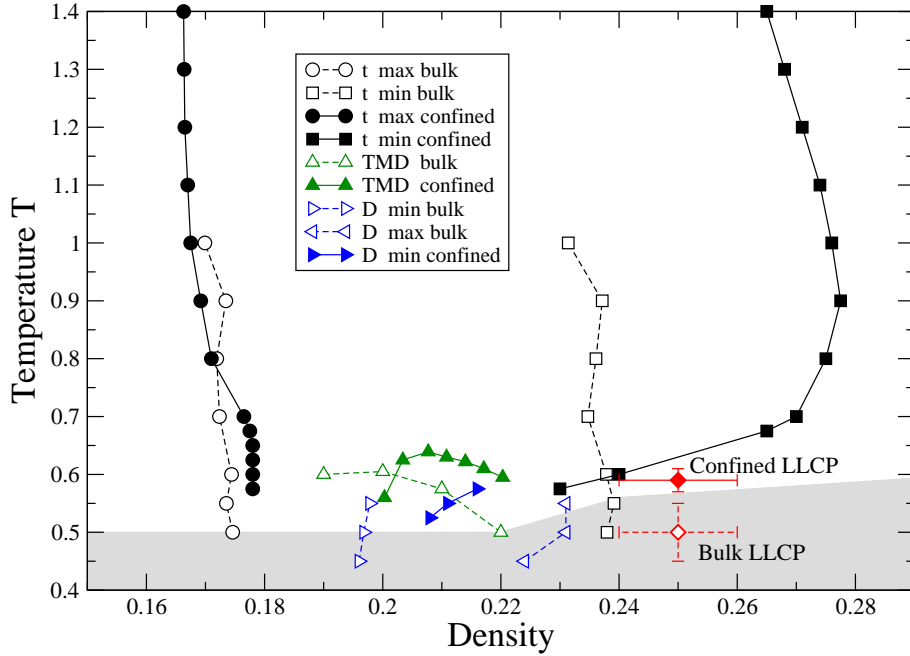


FIG. 9. Hierarchy of anomalies in the temperature-density plane for the homogeneous confined fluid compared to the bulk. Density for the confined homogeneous fluid (continuous lines and filled symbols) is ρ_{eff} and for the bulk (dashed lines and open symbols) is ρ . For the confined fluid the phase diagram at low T is inaccessible for the overall spontaneous crystallization due to heterogeneous nucleation near the attractive wall (occurring approximately within the region marked with grey shade). The LLCPC for the confined fluid (filled diamond) occurs above the inaccessible region, at higher T with respect to the bulk (open diamond). For the confined fluid we find that the anomalies have the same hierarchy as in bulk, with the structural-anomaly region (circles for t_{max} and squares for t_{min}) that includes the TMD (upper triangles) and the diffusion-anomaly region (right triangles). However, the anomaly regions for the confined system extend to higher density and T than for the bulk. For the confined system the anomalous diffusion ranges up to the filling up of the pore with the crystal phase preventing the direct observation of the locus of isothermal maximum D (left triangles).

structure and dynamics and where bulk-like properties could be hypothesized.

Here, in the first place, we test if the thermodynamic properties of the homogeneous fluid under confinement can be compared to those calculated for the entire pore including the heterogeneous fluid, because in experiments is difficult to separate the signals associated to the homogeneous and the heterogeneous parts. We find that the isotherms describing the entire fluid respect to the homogeneous liquid are shifted towards higher pressures, especially at lower densities. This effect is a consequence of the density heterogeneities induced by the layering near the walls and is stronger at lower density. Despite this difference, the phase diagram of the entire confined fluid is qualitatively similar to the one for the homogeneous confined fluid, with the presence of a LLCPC in both cases. Therefore our results support that from the experimental analysis of the entire confined fluid it is possible to extract, at least qualitative, information about the homogeneous fluid.

Next, we find that the phase diagram of the homogeneous confined fluid can be rescaled to that of the bulk. In particular, the LLCPC of the confined system is shifted to higher T with respect to the bulk, while its density and pressure are not affected in a significant way (Figs. 4, 9). Previous simulations of ST2 water confined in a slit-pores entirely hydrophilic show an increase of T and P of the LLCPC, while the hydrophobic confinement has the opposite effect [67]. Other simulations for anomalous fluids show that the LLCPC pressure increases while the LLCPC temperature decreases when the fluid is confined between attractive [21] or repulsive walls [60]. Here we do not find any relevant effect for P and an effect for T of the LLCPC that is similar to that found in Ref. [67]. We rationalize the difference of our results with the others as a consequence of our confinement that is attractive (hydrophilic) on one wall and repulsive (hydrophobic) on the other, giving rise to possible compensations among the different contributions of the walls.

The shift that we find for the phase diagram toward higher T is particularly relevant because the bulk LLCPC occurs at a temperature that would be not accessible in confinement for the inevitable heterogeneous nucleation induced by the attractive wall. Therefore, our result suggests that a mixed (attractive/repulsive) confinement could be helpful in

bringing the LLPT to a more experimentally accessible temperature.

Nevertheless, we observe that our slit-pore is large enough to include eleven layers of particles and that near the T of the LLCPC four/five of these layers are fluid. For water this would correspond to a wall-to-wall distance of ~ 3.3 nm. This distance is larger than the typical size of confining pores in experiments, 1.4 - 2.0 nm [24, 27, 29, 31], except that for the experiments performed by Zanotti et al. with water filled in Vycor 7930, which has 5 nm pore size [25, 68]. Because we find that the attractive wall induces the formation of approximately four layers of crystal/amorphous [53] at a temperature that is much ($\sim 40\%$) higher than the T of the bulk LLCPC, we expect that in hydrophilic slit pores separated by a few layers of water the LLCPC would be accessible only if it moves more than 40% up in temperature with respect to bulk. However, it is likely that, as in other models [21], the LLCPC would be preempted by crystallization in such a narrow slit pore [69]. Yet, our results support that in mild confinement, such as the one considered by Zanotti et al. [25] with ~ 15 layers of confined fluid it would be possible to observe the LLCPC at a T higher than for the bulk.

Next, we compute the TMD, the diffusion and the structural anomalies for the confined fluid. We find a shift of the anomalous regions towards larger densities and temperatures with respect to the bulk, while the hierarchical order is not altered. In particular, we observe that in both confined and bulk fluid the region with structural anomaly includes the TMD line and the region where the diffusion is anomalous. The full crystallization/amorphization of the fluid inside the slit pore at high density and low temperature prevents us from determining the high-density limit of the diffusion anomaly.

It is interesting to observe that the high-density limit of the structure anomaly for the confined case seems to be strongly correlated at low T to the filling up of the pore with the solid phase (Fig. 9). This observation suggests that the anomalous reduction of the translational order for increasing density could be the leading cause for the suppression of the crystal phase. Once the translational order recovers a normal behavior, at density higher than the locus of t_{\min} , the fluid starts to crystallize.

Our observations could help in interpreting experiments with confined anomalous fluids, and especially water, in which it is unclear if the fluid retains the thermodynamic properties of the bulk [70, 71]. Our result suggests that confined and bulk anomalous fluids can share the same thermodynamics, including the occurrence of the LLCPC, at the least when the pore size is more than ten times larger than a fluid layer, as in Ref. [25]. Furthermore, our study does not consider the effect of curvature of the confining walls on the crystallization rate. It is reasonable to hypothesize that the curvature would diminish the crystallization rate making the supercooled liquid accessible also in strong confinement, such as in Refs. [24, 27, 29, 31].

ACKNOWLEDGMENTS

We thank Marco Bernabei, Valentino Bianco, Carles Calero, David Reguera and Oriol Vilanova for useful discussions. We acknowledge the support of Spanish MINECO grant FIS2012-31025.

-
- [1] M.-C. Bellissent-Funel, S. H. Chen, and J.-M. Zanotti, *Phys. Rev. E* **51**, 4558 (1995).
 - [2] M. Schoen and D. J. Diestler, *J. Chem. Phys.* **109**, 5596 (1998).
 - [3] R. J. Mashl, S. Joseph, N. R. Aluru, and E. Jakobsson, *Nano Letters* **3**, 589 (2003).
 - [4] J. Mittal, T. M. Truskett, J. R. Errington, and G. Hummer, *Phys. Rev. Lett.* **100**, 145901 (2008).
 - [5] G. Cicero, J. C. Grossman, E. Schwegler, F. Gygi, and G. Galli, *J. Am. Chem. Soc.* **130**, 1871 (2008).
 - [6] A. De Virgiliis, R. L. C. Vink, J. Horbach, and K. Binder, *Phys. Rev. E* **78**, 041604 (2008).
 - [7] N. Giovambattista, P. J. Rossky, and P. G. Debenedetti, *J. Phys. Chem. B* **113**, 13723 (2009).
 - [8] S. R.-V. Castrillón, N. Giovambattista, I. A. Aksay, and P. G. Debenedetti, *J. Phys. Chem. B* **113**, 7973 (2009).
 - [9] S. R.-V. Castrillón, N. Giovambattista, I. A. Aksay, and P. G. Debenedetti, *J. Phys. Chem. B* **113**, 1438 (2009).
 - [10] R. Mancinelli, S. Imberti, A. K. Soper, K. H. Liu, C. Y. Mou, F. Bruni, and M. A. Ricci, *J. Phys. Chem. B* **113**, 16169 (2009).
 - [11] W. Rzyzko, A. Patrykiewicz, S. Sokolowski, and O. Pizio, *J. Chem. Phys.* **132**, 164702 (2010).
 - [12] S. Han, M. Y. Choi, P. Kumar, and H. E. Stanley, *Nature Phys.* **6**, 685 (2010).
 - [13] F. de los Santos and G. Franzese, *J. Phys. Chem. B* **115**, 14311 (2011).
 - [14] S. K. Schnell, T. J. H. Vlugt, J.-M. Simon, D. Bedeaux, and S. Kjelstrup, *Chem. Phys. Lett.* **504**, 199 (2011).
 - [15] S. K. Schnell, T. J. H. Vlugt, J.-M. Simon, D. Bedeaux, and S. Kjelstrup, *Mol. Phys.* **110**, 1069 (2011).
 - [16] R. R. Nair, H. A. Wu, P. N. Jayaram, I. V. Grigorieva, and A. K. Geim, *Science* **335**, 442 (2012).
 - [17] D. R. Paul, *Science* **335**, 413 (2012).
 - [18] A. L. Ferguson, N. Giovambattista, P. J. Rossky, A. Z. Panagiotopoulos, and P. G. Debenedetti, *J. Chem. Phys.* **137**, 144501 (2012).

- [19] M. C. Stewart and R. Evans, *Phys. Rev. E* **86**, 031601 (2012).
- [20] L. B. Krott and M. C. Barbosa, *J. Chem. Phys.* **138**, 084505 (2013).
- [21] G. Sun, N. Giovambattista, and L. Xu, *J. Chem. Phys.* **143** (2015).
- [22] R. Bergman and J. Swenson, *Nature* **403**, 283 (2000).
- [23] A. Faraone, L. Liu, C.-Y. Mou, C.-W. Yen, and S.-H. Chen, *J. Chem. Phys.* **121**, 10843 (2004).
- [24] L. Liu, S.-H. Chen, A. Faraone, C.-W. Yen, and C.-Y. Mou, *Phys. Rev. Lett.* **95**, 117802 (2005).
- [25] J. M. Zanotti, M. C. Bellissent-Funel, and S. H. Chen, *Europhys. Lett.* **71**, 91 (2005).
- [26] E. Mamontov, C. J. Burnham, S. H. Chen, A. P. Moravsky, C. K. Loong, N. R. de Souza, and A. I. Kolesnikov, *J. Chem. Phys.* **124**, 194703 (2006).
- [27] F. Mallamace, M. Broccio, C. Corsaro, A. Faraone, D. Majolino, V. Venuti, L. Liu, C.-Y. Mou, and S.-H. Chen, *Proc. Natl. Acad. Sci. USA* **104**, 424 (2007).
- [28] F. Mallamace, C. Corsaro, M. Broccio, C. Branca, N. González-Segredo, J. Spooren, S. H. Chen, and H. E. Stanley, *Proc. Natl. Acad. Sci. USA* **105**, 12725 (2008).
- [29] Y. Zhang, A. Faraone, W. A. Kamitakahara, K.-H. Liu, C.-Y. Mou, J. B. Leão, S. Chang, and S.-H. Chen, *Proc. Natl. Acad. Sci. USA* **108**, 12206 (2011).
- [30] A. Cupane, M. Fomina, and G. Schirò, *J. Chem. Phys.* **141**, 18C510 (2014).
- [31] A. Cupane, M. Fomina, I. Piazza, J. Peters, and G. Schirò, *Phys. Rev. Lett.* **113**, 215701 (2014).
- [32] L. Xu, P. Kumar, S. V. Buldyrev, S.-H. Chen, P. H. Poole, F. Sciortino, and H. E. Stanley, *Proc. Natl. Acad. Sci. USA* **102**, 16558 (2005).
- [33] M. Meyer and H. E. Stanley, *J. Phys. Chem. B* **103**, 9728 (1999).
- [34] P. Kumar, S. V. Buldyrev, F. W. Starr, N. Giovambattista, and H. E. Stanley, *Phys. Rev. E* **72**, 051503 (2005).
- [35] P. Gallo, M. Rovere, and S.-H. Chen, *J. Phys. Condens. Matter* **22**, 284102 (2010).
- [36] H. E. Stanley, S. V. Buldyrev, G. Franzese, P. Kumar, F. Mallamace, M. G. Mazza, K. Stokely, and L. Xu, *J. Phys. Condens. Matter* **22**, 284101 (2010).
- [37] E. G. Strelakova, M. G. Mazza, H. E. Stanley, and G. Franzese, *Phys. Rev. Lett.* **106**, 145701 (2011).
- [38] M. G. Mazza, K. Stokely, S. E. Pagnotta, F. Bruni, H. E. Stanley, and G. Franzese, *Proc. Natl. Acad. Sci. USA* (2011).
- [39] E. G. Strelakova, M. G. Mazza, H. E. Stanley, and G. Franzese, *J. Phys. Condens. Matter* **24**, 064111 (2012).
- [40] E. Strelakova, D. Corradini, M. Mazza, S. Buldyrev, P. Gallo, G. Franzese, and H. Stanley, *J. Biol. Phys.* **38**, 97 (2012-01-01).
- [41] E. G. Strelakova, J. Luo, H. E. Stanley, G. Franzese, and S. V. Buldyrev, *Phys. Rev. Lett.* **109**, 105701 (2012).
- [42] C. E. Bertrand, Y. Zhang, and S.-H. Chen, *Phys. Chem. Chem. Phys.* **15**, 721 (2013).
- [43] G. Pallares, M. El Mekki Azouzi, M. A. González, J. L. Aragonés, J. F. Abascal, C. Valeriani, and F. Caupin, *Proc. Natl. Acad. Sci. USA* **111**, 7936 (2014).
- [44] T. M. Truskett, P. G. Debenedetti, and S. Torquato, *J. Chem. Phys.* **114**, 2401 (2001).
- [45] K. Stokely, M. G. Mazza, H. E. Stanley, and G. Franzese, *Proc. Natl. Acad. Sci. U.S.A.* **107**, 1301 (2010).
- [46] A. K. Soper, *Proc. Natl. Acad. Sci. USA* **108**, E1192 (2011).
- [47] Y. Zhang, A. Faraone, W. A. Kamitakahara, K.-H. Liu, C.-Y. Mou, J. B. Leão, S. Chang, and S.-H. Chen, *Proc. Natl. Acad. Sci. USA* **108**, E1193 (2011).
- [48] A. K. Soper, *J. Phys. Condens. Matter* **24** (2012).
- [49] G. Franzese, *J. Mol. Liq.* **136**, 267 (2007).
- [50] A. B. de Oliveira, G. Franzese, P. A. Netz, and M. C. Barbosa, *J. Chem. Phys.* **128**, 064901 (2008).
- [51] P. Vilaseca and G. Franzese, *J. Chem. Phys.* **133**, 084507 (2010).
- [52] P. Vilaseca and G. Franzese, *J. Non-Cryst. Solids* **357**, 419 (2011).
- [53] F. Leoni and G. Franzese, *J. Chem. Phys.* **141**, 174501 (2014).
- [54] P. Vilaseca, K. A. Dawson, and G. Franzese, *Soft Matter* **9**, 6978 (2013).
- [55] M. Huš and T. Urbic, *Phys. Rev. E* **90**, 062306 (2014).
- [56] R. Ryltsev, B. Klumov, and N. Chitchev, *Soft Matter* **11**, 6991 (2015).
- [57] A. R. Denton and H. Löwen, *Phys. Rev. Lett.* **81**, 469 (1998).
- [58] Z. Yan, S. V. Buldyrev, P. Kumar, N. Giovambattista, and H. E. Stanley, *Phys. Rev. E* **77**, 042201 (2008).
- [59] M. Agarwal, M. Singh, R. Sharma, M. Parvez Alam, and C. Chakravarty, *J. Phys. Chem. B* **114**, 6995 (2010).
- [60] L. B. Krott, J. R. Bordin, N. M. Barraz, and M. C. Barbosa, *J. Chem. Phys.* **142**, 134502 (2015).
- [61] F. Varnik, J. Baschnagel, and K. Binder, *J. Chem. Phys.* **113**, 4444 (2000).
- [62] M. Schoen and S. Klapp, *Nanoconfined Fluids: Soft Matter Between Two and Three Dimensions*, volume 24 of *Reviews in Computational Chemistry*, chapter Appendix E: Mathematical Aspects of Monte Carlo simulations, pages 431–446, John Wiley & Sons, Inc., 2007.
- [63] M. P. Allen and D. J. Tildesley, *Computer simulation of liquids*, Oxford university press, 1989.
- [64] M. S. Shell, P. G. Debenedetti, and A. Z. Panagiotopoulos, *Phys. Rev. E* **66**, 011202 (2002).
- [65] J. R. Errington and P. D. Debenedetti, *Nature (London)* **409**, 318 (2001).
- [66] J. E. Errington, P. G. Debenedetti, and S. Torquato, *J. Chem. Phys.* **118**, 2256 (2003).
- [67] I. Brovchenko and A. Oleinikova, *J. Chem. Phys.* **126** (2007).
- [68] T. Takamuku, M. Yamagami, H. Wakita, Y. Masuda, and T. Yamaguchi, *J. Phys. Chem. B* **101**, 5730 (1997).
- [69] For a repulsive slit pore under the same conditions the formation of crystal/amorphous layers is reduced to two [53], then the 40% rise in the T of LLCP would be necessary for a wall-to-wall distance of four layers, ~ 1.2 nm for water.
- [70] A. K. Soper, *Mol. Phys.* **106**, 2053 (2008).

[71] M. A. Ricci, F. Bruni, and A. Giuliani, *Faraday Discuss.* **141**, 347 (2008).